Available online at www.sciencedirect.com
ScienceDirect
Journal of Colloid and Interface Science 321 (2008) 103–117
JOURNAL OF Colloid and Interface Science
www.elsevier.com/locate/jcis

Complex conductivity of water-saturated packs of glass beads

P. Leroy [a,1], A. Revil [b,c,*,2], A. Kemna [d,3], P. Cosenza [e], A. Ghorbani [e]

[a] *CNRS, Université Aix-Marseille III, Aix-en-Provence, France*
[b] *Department of Geophysics, Colorado School of Mines, Golden, CO 80401, USA*
[c] *LGIT (UMR 5559), CNRS, Université de Savoie, Equipe Volcan, Le Bourget-du-Lac, France*
[d] *Agrosphere (ICG 4), Forschungszentrum Jülich, Germany*
[e] *UMR 7619 Sisyphe, Université Pierre et Marie Curie, Paris 6, Paris, France*

Received 21 November 2007; accepted 22 December 2007

Available online 12 February 2008

Abstract

The low-frequency conductivity response of water-saturated packs of glass beads reflects a combination of two processes. One process corresponds to the polarization of the mineral/water interface coating the surface of the grains. The other process corresponds to the Maxwell–Wagner polarization associated with accumulation of the electrical charges in the pore space of the composite medium. A model of low-frequency conductivity dispersion is proposed. This model is connected to a triple-layer model of electrochemical processes occurring at the surface of silica. This model accounts for the partition of the counterions between the Stern and the diffuse layers. The polarization of the mineral/water interface is modeled by the electrochemical polarization model of Schurr for a spherical grain. We take into account also the DC surface conductivity contribution of protons of the sorbed water and the contribution of the diffuse layer. At the scale of a macroscopic representative elementary volume of the porous material, the electrochemical polarization of a single grain is convoluted with the grain size distribution of the porous material. Finally, the Maxwell–Wagner polarization is modeled using the complex conductivity of a granular porous medium obtained from the differential effective medium theory. The predictions of this model agree well with experimental data of spectral induced polarization. Two peaks are observed at low frequencies in the spectrum of the phase. The first peak corresponds to the distribution of the size of the beads and the second peak is due to the roughness of the grains.

Keywords: Spectral impedance; Porous media; Induced polarization; Complex conductivity; Double layer; Particle size distribution

1. Introduction

Complex conductivity appears a very promising method to image nonintrusively the three-dimensional distribution of the permeability of porous materials [1–5] and its evolution over time, to detect the presence of various types of contaminants in the ground [6], and to study the properties of colloidal suspensions in the laboratory [7–11]. The complex conductivity response of a water-saturated porous material usually exhibits relaxation phenomena in the frequency range extending from milliHertz to few kiloHertz [1,7–11]. Some researchers [12–14] have proposed phenomenological models, such as the Cole–Cole model, to fit the effective conductivity data in this frequency range. Whereas these models are very useful for practical applications, they do not relate the effective conductivity response to intrinsic physical and chemical properties of the porous medium.

Several studies have investigated the fundamental processes leading to the low-frequency dispersion of colloids. Two processes are known to be responsible for the observed data. One process is related to the polarization of the electrical double or triple layer coating the surface of the grains: the electrochemical (EC) contribution [15–17]. A fixed charge density is located at the surface of all minerals in contact with water. This fixed charge density is counterbalanced by the charge densities of the

* Corresponding author.
E-mail address: arevil@mines.edu (A. Revil).
[1] Present address: BRGM, Orléans, France.
[2] Also at CNRS-ANDRA/GDR FORPRO 0788, France.
[3] Present address: Department of Geodynamics and Geophysics, University of Bonn, Germany.

0021-9797/$ – see front matter
doi:10.1016/j.jcis.2007.12.031

Stern and diffuse layers. The theory of the low-frequency EC conductivity dispersion was first elaborated for dilute suspensions of homogeneous spherical insulating particles surrounded by a thin mineral/water interface [15–19]. In this case, the diffuse layer and/or the Stern layer and the electrolyte located in the vicinity of the interface become polarized. However, in a water-saturated granular porous material with a finite contiguity between the grains, the overlapping of the electrical diffuse layer at the grain-to-grain contacts probably impedes the polarization of the electrical diffuse layer (the electrical diffuse layer is above a percolation threshold of the material and therefore does not polarize). It follows that the electrochemical polarization may be due to the polarization of the Stern layer alone.

The theory of Schwarz [15] takes into account the diffusional relaxation of the counterion distribution along tangential concentration gradients in a conductive layer located at the surface of spherical insulating grains. This model is valid for a binary symmetric 1:1 electrolyte such as NaCl or KCl. Schurr [16] generalized the model of Schwarz by including the effects of DC surface conductivity. In this model, he partitioned the fixed charge layer into two parts: an inner layer, which was tightly bound to the particle surface, and an outer layer, which was loosely bound to the particle surface. Dukhin and Shilov [17] studied the flux of ions in thin double layers and the surrounding symmetric electrolyte. A quite similar analysis was provided later by Fixman [18], O'Brien [20], and Hinch et al. [21]. Lyklema et al. [19] modified the Schwarz theory to include the polarization of the diffuse layer but not the polarization of the surrounding electrolyte.

The other process needed to model the complex conductivity of a water-saturated porous material is the Maxwell–Wagner (MW) polarization [22,23]. In a porous composite, the different phases have different conductivities and dielectric constants. The MW polarization is caused by the formation of field-induced free charge distributions near the interface between the phases of the composite. In the case of granular media, models based on the effective medium approximation [24–26] have successfully modeled the Maxwell–Wagner polarization of a pack of spherical grains. A closed-form solution for the electrical conductivity response of a granular porous composite was introduced [27,28]. Note that because the diffuse and Stern layers modify the conductivity of micropores and grains, respectively, they also influence the MW polarization of saturated porous materials.

Recently, various researchers have combined the theories of the EC and MW polarizations to predict the complex dielectric responses of conductive porous media over a wide frequency range [29,30]. However, these models were not fully connected with an electrical triple-layer model (TLM) showing explicitly the role of the partition of the counterions between the Stern and the diffuse layers. Because the value of the partition coefficient describing the distribution of the counterions between the Stern and the diffuse layers depends on the ionic strength of the pore water, its composition, and its pH, this partition coefficient needs to be considered explicitly in polarization models. It is therefore crucial to combine the EC polarization models with an electrical double- or triple-layer model that accounts for the complexation between the ions in the pore water solution and the active sites covering the surface of the mineral.

In this paper, we propose a model of low-frequency conductivity dispersion accounting for both electrochemical and Maxwell–Wagner polarizations, including a full connection to the electrical triple-layer model, and accounting for the grain size distribution of the porous material. This model was tested against experimental data.

2. Electrical triple-layer model

We consider silica grains in contact with a binary symmetric electrolyte such as NaCl for the simplicity of the presentation and the comparison with the experimental data. In the pH range 4–10, the surface mineral reactions at the silanol surface sites can be written as follows (see [31,32]):

$$>\mathrm{SiO^-} + \mathrm{H^+} \Leftrightarrow >\mathrm{SiOH}, \quad K_1, \tag{1}$$

$$>\mathrm{SiOH} + \mathrm{H^+} \Leftrightarrow >\mathrm{SiOH_2^+}, \quad K_2, \tag{2}$$

and

$$>\mathrm{SiO^-} + \mathrm{Na^+} \Leftrightarrow >\mathrm{SiONa}, \quad K_3. \tag{3}$$

The symbol $>$ refers to the mineral framework and K_1, K_2, and K_3 are the associated equilibrium constants for the different reactions reported above. Additional reactions for a multicomponent electrolyte can be easily incorporated by adding reactions similar to Eq. (3) or exchange reactions [33]. Therefore the present model is not limited to a binary salt. The protonation of surface siloxane groups $>\mathrm{SiO_2}$ is extremely low and these groups can be considered inert [34]. We neglect here the adsorption of anion $\mathrm{Cl^-}$ at the surface of the $>\mathrm{SiOH_2^+}$ sites which occurs at $\mathrm{pH} < \mathrm{pH(pzc)} \approx 2$–3 [35], where pzc is the point of zero charge of silica:

$$\mathrm{pH(pzc)} = \frac{1}{2}(\log K_1 + \log K_2). \tag{4}$$

Consequently, K_2 is determined from the value of K_1 and the value of the pH of the zero point of charge. In addition, we have $\mathrm{pH(pzc)} \approx 3$.

We develop an electrical TLM to determine the distribution of the coions and counterions at the mineral/water interface of silica minerals. The surface charge density Q_0 (in $\mathrm{C\,m^{-2}}$) at the surface of the minerals (see Fig. 1) can be expressed as

$$Q_0 = e\left(\Gamma^0_{\mathrm{SiOH_2^+}} - \Gamma^0_{\mathrm{SiO^-}} - \Gamma^0_{\mathrm{SiONa}}\right), \tag{5}$$

where Γ_i^0 is the surface site density of species i (in sites $\mathrm{m^{-2}}$). The sites $>\mathrm{SiONa}$ contribute to Q_0 in Eq. (5) because they are actually $>\mathrm{SiO^-Na^+}$ sites with $>\mathrm{SiO^-}$ located on the surface of the mineral and $\mathrm{Na^+}$ located in the Stern layer (see Eq. (6) below). The surface charge density Q_β in the Stern layer is determined according to

$$Q_\beta = e\Gamma^0_{\mathrm{SiONa}}. \tag{6}$$

The surface charge density in the diffuse layer is calculated using the classical Gouy–Chapman relationship in the case of a

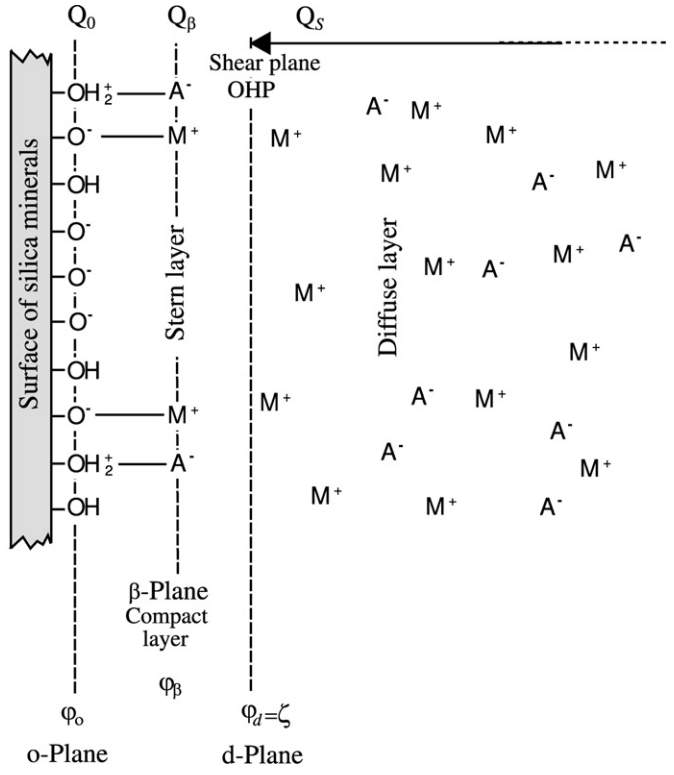

Fig. 1. Sketch of the electrical triple-layer model as suggested by Davis and Leckie [42]. M represents the metal cations (e.g., Na^+ or K^+) and A the anions (e.g., Cl^-). OHP represents the outer Helmholtz plane, which corresponds here to the shear plane where the zeta potential is defined. Q_0 is the surface charge density of the surface of the mineral, Q_β is the surface charge density of the Stern layer, and Q_S is the equivalent surface charge density of the diffuse layer.

symmetric monovalent electrolyte [36],

$$Q_S = -\sqrt{8\varepsilon_f k_b T C_f}\sinh(e\varphi_d/2k_bT), \tag{7}$$

where C_f is the salinity in the free electrolyte (in $\mathrm{mol\,L^{-1}}$), T is the temperature (in K), ε_f is the permittivity of the pore water ($\varepsilon_f = 81\varepsilon_0$, $\varepsilon_0 \sim 8.85\times10^{-12}\,\mathrm{F\,m^{-1}}$), e represents the elementary charge (taken positive, $e = 1.6\times10^{-19}$ C), and k_b is the Boltzmann constant ($1.381\times10^{-23}\,\mathrm{J\,K^{-1}}$). The electrical potential φ_d (in V) is the electrical potential at the outer Helmholtz plane (OHP; see Fig. 1). We make the assumption that the electrical potential φ_d is equal to the zeta potential ζ placed at the shear plane. The shear plane is the hydrodynamic surface on which the relative velocity between the mineral grains and the pore water is null [37].

The continuity equation for the surface sites yields

$$\Gamma_1^0 = \Gamma_{\mathrm{SiO^-}}^0 + \Gamma_{\mathrm{SiOH}}^0 + \Gamma_{\mathrm{SiOH_2^+}}^0 + \Gamma_{\mathrm{SiONa}}^0, \tag{8}$$

where Γ_1^0 (in $\mathrm{sites\,m^{-2}}$) is the total surface site density of the mineral. We use the equilibrium constants associated with the half-reactions to calculate the surface site densities Γ_i^0. Solving Eq. (8) with the expressions of the equilibrium constants defined through Eqs. (1) to (3) yields

$$\Gamma_{\mathrm{SiO^-}}^0 = \Gamma_1^0/A, \tag{9}$$

$$\Gamma_{\mathrm{SiOH}}^0 = \frac{\Gamma_1^0}{A}K_1 C_{\mathrm{H^+}}^f \exp\left(-\frac{e\varphi_0}{k_bT}\right), \tag{10}$$

$$\Gamma_{\mathrm{SiOH_2^+}}^0 = \frac{\Gamma_1^0}{A}K_1K_2 C_{\mathrm{H^+}}^{f^2} \exp\left(-\frac{2e\varphi_0}{k_bT}\right), \tag{11}$$

$$\Gamma_{\mathrm{SiONa}}^0 = \frac{\Gamma_1^0}{A}K_3 C_{\mathrm{Na^+}}^f \exp\left(-\frac{e\varphi_\beta}{k_bT}\right), \tag{12}$$

and

$$A = 1 + K_1 C_{\mathrm{H^+}}^f \exp\left(-\frac{e\varphi_0}{k_bT}\right) + K_1K_2 C_{\mathrm{H^+}}^{f^2} \exp\left(-\frac{2e\varphi_0}{k_bT}\right) + K_3 C_{\mathrm{Na^+}}^f \exp\left(-\frac{e\varphi_\beta}{k_bT}\right), \tag{13}$$

where φ_0 and φ_β are, respectively, the electrical potential at the o-plane corresponding to the mineral surface and the electrical potential at the β-plane corresponding to the plane of the Stern layer (Fig. 1). The symbols $C_{\mathrm{H^+}}^f$ and $C_{\mathrm{Na^+}}^f$ represent the concentrations of the protons and the sodium cations in the free electrolyte. The electrical potentials are related by

$$\varphi_0 - \varphi_\beta = Q_0/C_1 \tag{14}$$

and

$$\varphi_\beta - \varphi_d = -Q_S/C_2 \tag{15}$$

[36], where C_1 and C_2 (in $\mathrm{F\,m^{-2}}$) are the (constant) integral capacities of the inner and outer parts of the Stern layer, respectively. The global electroneutrality equation for the mineral/water interface is

$$Q_0 + Q_\beta + Q_S = 0. \tag{16}$$

We calculate the φ_d potential using Eqs. (5) to (16) and the procedure reported in [33,38]. We use $\Gamma_1^0 = 5\ \mathrm{sites\,nm^{-2}}$ [39,40] and $C_2 = 0.2\ \mathrm{F\,m^{-2}}$ [40–42]. We use the values of K_1, K_3, and C_1 given by Bolt [43] (see these values at Figs. 2a and 2b) to calculate the surface charge density Q_0 at the surface of silica mineral and the potential φ_d. Figs. 2 and 3 show good agreement between measured charge densities and zeta potentials and the model at various pHs and salinities.

As shown above, the counterions are located in both the Stern and the diffuse layers. The fraction of counterions located in the Stern layer is defined by

$$f_Q = \frac{\Gamma_{\mathrm{SiONa}}^0}{\Gamma_{\mathrm{SiONa}}^0 + \Gamma_{\mathrm{Na}}^d}, \tag{17}$$

$$\Gamma_{\mathrm{Na}}^d \equiv \int_0^\infty \left[C_{\mathrm{Na^+}}^d(r) - C_{\mathrm{Na^+}}^f\right]\mathrm{d}r = C_{\mathrm{Na^+}}^f \int_0^\infty \left\{\exp\left[-\frac{e\varphi(r)}{k_bT}\right] - 1\right\}\mathrm{d}r, \tag{18}$$

and

$$\varphi(r) = \frac{4k_bT}{e}\tanh^{-1}\left[\tanh\left(\frac{e\varphi_d}{4k_bT}\right)\exp(-\kappa r)\right], \tag{19}$$

where r is the local distance defined perpendicularly from the interface between the pore water and the solid grain, φ is the

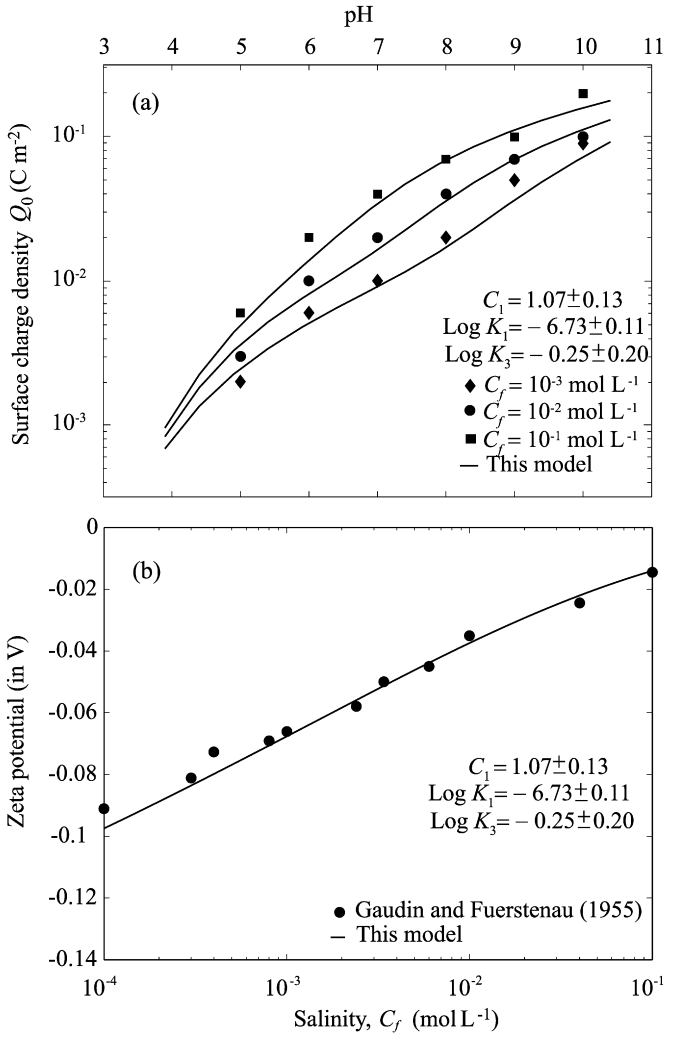

Fig. 2. Comparison between the predictions of the TLM model and the experimental data in the case of silica minerals. (a) Comparison between the prediction of the model and the surface charge density measurements obtained by potentiometric titrations at three different salinities (NaCl) and in the pH range 5–10 (data from [31]). (b) Comparison between the model prediction and the measurements of the zeta potential at different salinities and pH 6.5 (data from [61]). C_1 is expressed in F m^{-2}.

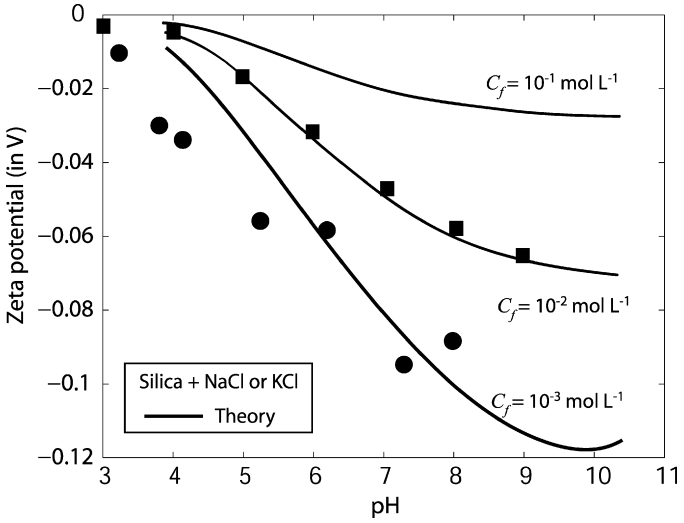

Fig. 3. Zeta potential versus pH at different background pore water salinities (NaCl). Data: filled squares (pure silica, 10^{-2} M NaCl, from streaming potential measurements); filled circles (glass beads, 10^{-3} M NaCl) (data from [56], streaming potential measurements).

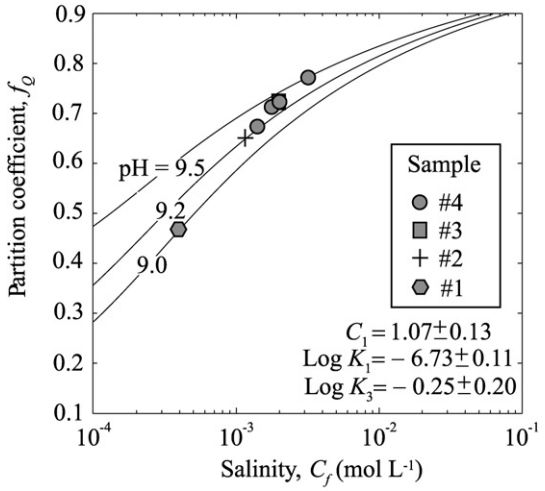

Fig. 4. Partition coefficient versus salinity of the free electrolyte with the TLM parameters indicated in Fig. 2 for NaCl (pH 9, 9.2, 9.5). The symbols correspond to the partition coefficient determined from the complex conductivity data for the seven experiments described in the main text. The data show an increase of the partition coefficient with the salinity and the pH in fair agreement with the model. C_1 is expressed in F m^{-2}.

electrical potential in the diffuse layer, κ^{-1} is the Debye screening length (in m) ($2\kappa^{-1}$ corresponds approximately to the thickness of the diffuse layer; see [32]), and Γ^d_{Na} is the equivalent surface density of the counterions in the diffuse layer. Equation (19) can be found for example in Hunter [36]. The superscript d for the bulk concentration and surface density of sodium refers to the diffuse layer. In the next section, we will replace $\Gamma^0_{\mathrm{SiONa}}$ by Γ^S_{Na} to denote the surface concentration of counterions in the Stern layer.

Fig. 4 shows that the fraction of counterions located in the Stern layer depends strongly on the salinity and the pH of the solution. For example, at pH 9 and at low salinities ($\leqslant 5 \times 10^{-4}$ mol L^{-1}) most of the counterions are located in the diffuse layer whereas at high salinity ($> 5 \times 10^{-4}$ mol L^{-1}) the counterions are located mainly in the Stern layer. At pH 9.5, most of the counterions are adsorbed in the Stern layer.

3. Electrochemical polarization

As discussed in Section 2, the electrical double or triple layer comprises the Stern and the diffuse layers. The Stern layer is sometimes divided into two sublayers. These layers, coating a grain, are polarized when the grains are submitted to an alternating electric field. The polarization of the electrical double layer corresponds to the so-called EC polarization of the medium [19]. We first consider the case of a single spherical silica grain with a homogeneous charged surface and a thin diffuse layer satisfying the condition $a_0 \gg 2\kappa^{-1}$, where a_0 is the radius of the particle (expressed in meters and where κ^{-1} is the Debye screening length). We restrict ourselves to the polariza-

tion of the Stern layer and will not consider the polarization of the diffuse layer. Indeed, in a granular porous material with a small grain-to-grain contiguity, the overlapping of the electrical diffuse layer at the grain-to-grain contacts prevents its polarization. Therefore we believe that models based on the polarization of the diffuse layer do not represent correctly the EC polarization of a granular porous medium whereas these models are correct for a dilute suspension of grains with no contiguity between the grains. In Section 3.2, we will convolve the response obtained for a single grain size with the particle size distribution of the porous material.

3.1. Polarization of the Stern layer

A porous material made of spherical silica grains of radius a_0 is saturated by an electrolyte solution comprising M species. We note $q_i = \pm e z_i$, the charge of species i (expressed in C), where z_i is the valence of species i. We denote C_i (in $\mathrm{mol\,L^{-1}}$) the concentration of species i (number of ions per unit pore volume). We consider an oscillating electrical field with magnitude $E_0 = |\mathbf{E}_0|$ and

$$\mathbf{E} = -\nabla\psi = \mathbf{E}_0 \exp(i\omega t), \tag{20}$$

where $i^2 = -1$ and ω is the angular frequency. Note that the electrical potential ψ due to the applied (external) electrical field is different from the electrical potential φ resulting in the electrical double layer. The superposition principle yields $\psi + \varphi$ for the total electrical potential in the pore space. The electrical potential ψ and the ionic concentrations C_i^f in the pore fluid are related by the Poisson equation, which combines Gauss's law and the Boltzmann distribution for the ionic concentrations:

$$\nabla \cdot (\varepsilon_f \nabla\psi) = -\sum_{i=1}^{M} q_i C_i^f. \tag{21}$$

In Eq. (21) the concentrations of the ionic species are described by Boltzmann distributions in the Coulombic field created by the charge density existing at the surface of the mineral. In the diffuse layer, the Poisson equation connects the electrical potential φ with the volumetric charge density $\bar{Q}_V$ (in $\mathrm{C\,m^{-3}}$):

$$\nabla \cdot (\varepsilon_f \nabla\varphi) = -\bar{Q}_V. \tag{22}$$

The volumetric charge density per unit pore volume $\bar{Q}_V$ is related to the partition coefficient f_Q by [44],

$$\bar{Q}_V = (1 - f_Q) Q_V, \tag{23}$$

where Q_V represents the total bulk charge density corresponding to the excess of charge per unit pore volume of the porous material. For clays, this is this bulk charge density that can be obtained from cation exchange capacity measurements.

The complex effective conductivities of the particle and of the surrounding electrolyte are defined by

$$\sigma_s^* = \sigma_s + i\omega\varepsilon_s \tag{24}$$

and

$$\sigma_f^* = \sigma_f + i\omega\varepsilon_f. \tag{25}$$

The variables σ_s, σ_f, ε_s, and ε_f are the conductivities (in $\mathrm{S\,m^{-1}}$) and the dielectric permittivities of the particle (s) and the fluid (f), respectively.

We consider now a species i adsorbed onto the mineral surface. The boundary condition at the surface of the grain is given by the integration of Gauss's law over a small pillbox enclosing the charged surface [16],

$$\varepsilon_s \frac{\partial\psi_s}{\partial r}\bigg|_{a_0} - \varepsilon_f \frac{\partial\psi_f}{\partial r}\bigg|_{a_0} = q_i \bar{\Gamma}_i^S + Q_{\mathrm{DC}}, \tag{26}$$

where the subscripts s and f refer, respectively, to the electrical properties inside and outside the particle. The spherical coordinates r and θ are defined with $r = 0$ at the center of the grain and $\theta = 0$ in the direction of the electrical field. The expression containing $q_i \overline{\Gamma}_i^S$ (in $\mathrm{C\,m^{-2}}$) is the deviation of the surface charge density of bound counterions in the Stern layer from its value in thermodynamic equilibrium. The parameter Q_{DC} denotes the surface charge density produced by divergent DC currents and due to the counterions in the diffuse layer and the protons of the water sorbed onto the mineral surface [32].

Schwarz [15] stated that the free charge transported to the surface of the sphere by normal currents may not respond to tangential electric fields. He considered only the diffusive flux of counterions in a spherical ionic atmosphere and no exchange of charges between the bound layer of counterions and the electrolyte. A previous theory by O'Konski [45] took into account the surface conductance, which was considered independent of frequency over the region of the low-frequency dispersion. O'Konski [45] introduced an integral surface conductivity operating at the solid/solution interface to represent its excess electrical conduction. He also considered a free exchange of charges between the surface layer and the electrolyte, but he neglected the ionic diffusion around the surface of the particle.

Schurr [16] combined the treatments of Schwarz and O'Konski and distinguished the bound charge current, which is defined as that which is completely canceled by the current due to chemical potential gradients in the steady state and the DC current which persists in accordance with Ohm's law in the steady state. In Schurr's theory, the ionic atmosphere around a charged sphere immersed in an aqueous electrolyte is divided into two parts: one represents a thin layer of counterions tightly bound to the particle surface as in the Schwarz model ("fixed layer") and another represents the diffuse layer. The counterions in the thin layer move tangentially to the surface. The diffuse layer charges exchange readily with the bulk electrolyte. There is no polarization of the diffuse layer and there is no exchange of ions between the Stern and the diffuse layer.

Far away from the grain (outside the electrical diffuse layer), the ionic concentrations approach their bulk values and the electrical field is equal to the applied electrical field:

$$C_i \to C_i^f \quad \text{as } r \to \infty \tag{27}$$

and

$$\nabla\psi = -\mathbf{E} \quad \text{as } r \to \infty. \tag{28}$$

The ionic flux density $\mathbf{j}_i$ (in $\mathrm{mol\,m^{-2}\,s^{-1}}$) generated by the fluid velocity $\mathbf{v}_w$ (in $\mathrm{m\,s^{-1}}$) and by the electrochemical potential gra-

dient $\nabla\tilde{\mu}_i$ is given by the Nernst–Planck equation

$$\mathbf{j}_i = C_i\mathbf{v}_w - \ell_{ii}\nabla\tilde{\mu}_i, \tag{29}$$

where ℓ_{ii} is a phenomenological coefficient (the terms ℓ_{ij} $(i \neq j)$ represent interaction terms that are important only at high ionic strengths [46]). Equation (29) includes a convective term and an electrodiffusive term. We will consider the Coulombic interaction in the definition of the electrochemical potentials. This yields

$$\mathbf{j}_i = C_i\mathbf{v}_w - \frac{\beta_i C_i}{|q_i|}\nabla\tilde{\mu}_i, \tag{30}$$

where β_i is the mobility of species i (in $\mathrm{m^2\,s^{-1}\,V^{-1}}$) and $\mathbf{v}_w$ is the velocity of the fluid. The motion of the fluid results from electroosmotic coupling [63]. The gradient of the electrochemical potential of species i is defined by

$$\nabla\tilde{\mu}_i = k_bT\nabla\ln C_i + q_i\nabla\psi. \tag{31}$$

The counterions in the Stern layer are assumed to be able to move tangentially along the Stern layer. However, they are also assumed to be unable to enter or leave the Stern layer. This implies

$$\mathbf{j}_i\cdot\mathbf{n} = 0 \quad \text{at } r = a_0, \tag{32}$$

where $\mathbf{n}$ is the unit vector normal to the surface of the grain. In absence of chemical reactions with the mineral surface, the local continuity equation for the species i is

$$\nabla\cdot\mathbf{j}_i = -\frac{\partial C_i}{\partial t}. \tag{33}$$

Schwarz [15] assumed that, when an electrical field is applied to a spherical grain in solution, the charges in the fixed layer will migrate only in a direction tangential to the particle surface. From Eqs. (30) and (31), the flux of counterions is due to electromigration and diffusion. In spherical coordinates (with the center of the coordinate system at the center of a spherical grain), this flux is given by

$$j_i = -\frac{D_i^S}{a_0}\frac{\partial\Gamma_i^S}{\partial\theta} - \frac{\beta_i^S q_i\Gamma_i^S}{|q_i|a_0}\frac{\partial\psi_S}{\partial\theta}, \tag{34}$$

where the subscript or superscript S refers to the Stern layer, the diffusion coefficient of species i (in $\mathrm{m^2\,s^{-1}}$) is related to the mobility of this species by the Nernst–Einstein relationship $D_i^S = k_bT\beta_i^S/|q_i|$, and Γ_i^S is the concentration of species i in the Stern layer (in ions $\mathrm{m^{-2}}$).

The variation of the surface concentration of bound counterions Γ_i^S can be due solely to electromigration within the electrical field and diffusion in a tangential direction. This implies according to Eqs. (33) and (34) and in spherical coordinates

$$\frac{1}{a_0^2\sin\theta}\frac{\partial}{\partial\theta}\left(D_i^S\sin\theta\frac{\partial\Gamma_i^S}{\partial\theta} + \frac{\beta_i^S q_i\Gamma_i^S}{|q_i|}\sin\theta\frac{\partial\psi_S}{\partial\theta}\right) = \frac{\partial\Gamma_i^S}{\partial t}. \tag{35}$$

As stated by Schwarz [15], the applied electrical field does not deform the "fixed charge" at the surface of the particle. Consequently, the deviation of the surface concentration of bound ions from its value in thermodynamic equilibrium is very small:

$$\bar{\Gamma}_i^S(\theta,t) = \Gamma_i^S(\theta,t) - \Gamma_i^{S0} \ll \Gamma_i^{S0}. \tag{36}$$

Equation (35) can be linearized to the form

$$\frac{D_i^S}{a_0^2\sin\theta}\frac{\partial}{\partial\theta}\left(\sin\theta\frac{\partial\bar{\Gamma}_i^S}{\partial\theta} + \frac{q_i\Gamma_i^{S0}}{k_bT}\sin\theta\frac{\partial\psi_S}{\partial\theta}\right) = \frac{\partial\bar{\Gamma}_i^S}{\partial t}. \tag{37}$$

The DC current conduction is supposed to be independent of the bound charge polarization when the condition in Eq. (36) is satisfied. The DC surface conductivity Σ_S^0 resulting from electromigration in the diffuse layer and from the protons of the water adsorbed onto the mineral surface [32,45] is given by

$$\Sigma_S^0 = \int_{a_\zeta}^{2\kappa^{-1}} \big(\sigma_f(r) - \sigma_f\big)\,\mathrm{d}r + \Sigma_S^0(\mathrm{H^+}) \tag{38}$$

and

$$\Sigma_S^0 = e\sum_{i=1}^{N}\beta_i^f\Gamma_i^d + \Sigma_S^0(\mathrm{H^+}), \tag{39}$$

where the subscript or superscript f refers to the electrolyte with conductivity σ_f (in $\mathrm{S\,m^{-1}}$) and N is the number of species of counterions adsorbed onto the surface. In Eq. (38), $\sigma_f(r)$ is the local value of the conductivity of the pore water at distance r from the surface of the grains while σ_f is the electrical conductivity of the free pore water $\sigma_f = \sigma_f(r \gg 2k^{-1})$. We restrict ourselves now to the case where there are only counterions in the diffuse layer. In the following, we will suppose also that only cations exist at the mineral/water interface. The position a_ζ represents the position between the Stern and the diffuse layer around a spherical grain taken from the center of the grain. The density Γ_i^d is the surface site density of adsorbed counterions in the diffuse layer in the equilibrium state,

$$\Gamma_i^d \equiv \int_0^\infty \big[C_i^d(r) - C_i^f\big]\,\mathrm{d}r \tag{40}$$

and

$$\Gamma_i^d = C_i^f\int_0^\infty\left\{\exp\left[-\frac{q_i\varphi(r)}{k_bT}\right] - 1\right\}\mathrm{d}r, \tag{41}$$

where the electrical potential in the diffuse layer is given by Eq. (19).

The charge transport equation for the DC current is given by O'Konski [45]:

$$\frac{\Sigma_S^0}{a_0^2\sin\theta}\frac{\partial}{\partial\theta}\left(\sin\theta\frac{\partial\psi_S}{\partial\theta}\right) + \sigma_f\frac{\partial\psi_f}{\partial r}\bigg|_{a_0} - \sigma_s\frac{\partial\psi_s}{\partial r}\bigg|_{a_0} = \frac{\partial Q_{\mathrm{DC}}}{\partial t}. \tag{42}$$

The potential ψ_S must be derived from boundary conditions and the conservation equation for the electrical charge. The potential in the electrolyte ψ_f and the potential inside the sphere ψ_s satisfy the Laplace equation:

$$\nabla^2\psi_f = 0 \quad \text{for } r > a_0 \tag{43}$$

and

$$\nabla^2\psi_s = 0 \quad \text{for } r < a_0. \tag{44}$$

The boundary conditions are

$$\psi_s \quad \text{finite for } r \to 0, \tag{45}$$

$$\lim_{r\to a_0} \psi_f = \lim_{r\to a_0} \psi_s = \psi_S, \tag{46}$$

$$\psi_f \to -E_{0r}\cos\theta\exp(i\omega t) \quad \text{for } r \to \infty, \tag{47}$$

where E_{0r} is the radial component of $\mathbf{E}_0$, and

$$\varepsilon_s \frac{\partial\psi_s}{\partial r}\bigg|_{a_0} - \varepsilon_f \frac{\partial\psi_f}{\partial r}\bigg|_{a_0} = q_i\bar{\Gamma}_i^S + Q_{\mathrm{DC}} \quad \text{for } r = a_0. \tag{48}$$

The deviation of the surface concentration of bound ions from its value in thermodynamic equilibrium and the electrical potential ψ_S are determined using Eqs. (35)–(48) and Legendre polynomials. We restrict ourselves now to the case of a binary monovalent electrolyte such as NaCl (or KCl). Equation (37) leads to the following relationship between $\bar{\Gamma}^S_{\mathrm{Na}^+}$ and ψ_S (see [15]):

$$\bar{\Gamma}^S_{\mathrm{Na}^+} = -\frac{e\Gamma^{S0}_{\mathrm{Na}^+}}{(1+i\omega\tau^0_{\mathrm{Na}^+})k_bT}\psi_S \tag{49}$$

and

$$\tau^0_{\mathrm{Na}^+} = \frac{a_0^2}{2D^S_{\mathrm{Na}^+}}. \tag{50}$$

The relaxation time $\tau^0_{\mathrm{Na}^+}$ (in s) is calculated using the known diffusion coefficients of the counterions in the Stern layer $D^S_{\mathrm{Na}^+}$ (in $\mathrm{m^2\,s^{-1}}$).

The total current density $\mathbf{j}_S$ due to the movements of counterions in the Stern layer is defined by

$$\mathbf{j}_S = e\mathbf{j}^S_{\mathrm{Na}^+}. \tag{51}$$

The flux of counterions is determined by the following expression in spherical coordinates:

$$j^S_{\mathrm{Na}^+} = -\frac{\beta^S_{\mathrm{Na}^+}k_bT}{ea_0}\left(\frac{\partial\Gamma^S_{\mathrm{Na}^+}}{\partial\theta} + \frac{e\Gamma^S_{\mathrm{Na}^+}}{k_bT}\frac{\partial\psi_S}{\partial\theta}\right). \tag{52}$$

According to Eqs. (49) and (52) and using the assumptions $\partial\Gamma^S_{\mathrm{Na}^+}/\partial\theta \cong \partial\bar{\Gamma}^S_{\mathrm{Na}^+}/\partial\theta$ and $\Gamma^S_{\mathrm{Na}^+} \cong \Gamma^{S0}_{\mathrm{Na}^+}$, we obtain

$$j_S = -\frac{1}{a_0}\beta^S_{\mathrm{Na}^+}e\Gamma^{S0}_{\mathrm{Na}^+}\left(\frac{i\omega\tau^0_{\mathrm{Na}^+}}{1+i\omega\tau^0_{\mathrm{Na}^+}}\right)\frac{\partial\psi_S}{\partial\theta}, \tag{53}$$

$$\mathbf{j}_S = \beta^S_{\mathrm{Na}^+}e\Gamma^{S0}_{\mathrm{Na}^+}\left(\frac{i\omega\tau^0_{\mathrm{Na}^+}}{1+i\omega\tau^0_{\mathrm{Na}^+}}\right)\mathbf{e}_S, \tag{54}$$

and

$$\mathbf{j}_S = \Sigma^*_S\mathbf{e}_S, \tag{55}$$

where the local electrical field $\mathbf{e}_S = -(1/a_0)(\partial\psi_S/\partial\theta)\mathbf{t}_S$ ($\mathbf{t}_S$ is one of the two unit vectors that are tangential to the surface of the grain), Σ^*_S is the complex surface conductivity (sometimes called the complex surface conductance because it is expressed in Siemens) due to the fluxes of counterions in the Stern layer:

$$\Sigma^*_S = \beta^S_{\mathrm{Na}^+}e\Gamma^{S0}_{\mathrm{Na}^+}\left(\frac{i\omega\tau^0_{\mathrm{Na}^+}}{1+i\omega\tau^0_{\mathrm{Na}^+}}\right). \tag{56}$$

In the case of insulating spherical particles coated by a conductive and fixed layer, the complex conductivity of the particle is determined using Eqs. (56) and (42)–(48). This yields

$$\sigma^*_s = i\omega\varepsilon_s + \sigma_s, \tag{57}$$

$$\sigma_s = \frac{2(\Sigma^*_S + \Sigma^0_S)}{a_0}, \tag{58}$$

$$\sigma_s = \frac{2}{a_0}\left[\beta^S_{\mathrm{Na}^+}e\Gamma^{S0}_{\mathrm{Na}^+}\left(\frac{i\omega\tau^0_{\mathrm{Na}^+}}{1+i\omega\tau^0_{\mathrm{Na}^+}}\right) + \beta^S_{\mathrm{Na}^+}e\Gamma^d_{\mathrm{Na}^+} + \Sigma^0_S(\mathrm{H}^+)\right], \tag{59}$$

and

$$\Sigma^0_S = \beta^S_{\mathrm{Na}^+}e\Gamma^d_{\mathrm{Na}^+} + \Sigma^0_S(\mathrm{H}^+), \tag{60}$$

where Σ^0_S is the DC specific surface conductivity and $\Sigma^0_S(\mathrm{H}^+)$ is a contribution from the protons of the water adsorbed onto the mineral surface (see Revil and Glover [32] who give $\Sigma^0_S(\mathrm{H}^+) = 2.4\times10^{-9}$ S at 25 °C).

If there is only one characteristic relaxation time (one specific adsorption mechanism), one can rewrite Eq. (59) as

$$\sigma_s = \frac{2}{a_0}\left(\Sigma^0_S + \Sigma^\infty_S\right) - \frac{2}{a_0}\frac{\Sigma^\infty_S}{(1+i\omega\tau_0)} \tag{61}$$

and

$$\Sigma^\infty_S = \beta^S_{\mathrm{Na}^+}e\Gamma^{S0}_{\mathrm{Na}^+}, \tag{62}$$

where Σ^∞_S is the contribution of the Stern layer at high frequencies ($\omega \gg \tau_0^{-1}$). Equation (61) is similar to an equation used by [29].

3.2. Convolution with the particle size distribution

If the porous material is characterized by a particle size distribution (PSD), the effective surface conductivity is obtained by the convolution of the PSD with the conductivity response obtained for a Dirac distribution of grain size as a result of the superposition principle [47]

$$\sigma^*_s = f(a) \otimes \sigma^*_s(a,\omega) \tag{63}$$

and

$$\sigma^*_s = \sum_{i=1}^{Q} f(a_i)\sigma^*_s(a_i,\omega), \tag{64}$$

where $\otimes$ is the convolution product, a_i is the particle radius of the grain i, Q is the number of classes in the grain size distribution, and $f(a_i)$ represents the discretized version of the PSD $f(a)$. The total grain volume distribution is normalized to

unity:

$$\int_0^\infty f(a')\,\mathrm{d}a' = 1 \tag{65}$$

and

$$\sum_{i=1}^{Q} f(a_i) = 1. \tag{66}$$

This behavior can also be connected with the so-called Cole–Cole distribution widely used to represent the dispersive electrical properties of porous media [12,48]. In dealing with the dispersive complex surface conductivity function, we can write

$$\sigma_s^*(\omega) = \sigma_s^\infty + \left(\sigma_s^0 - \sigma_s^\infty\right) \int_0^\infty \frac{f(\tau)}{1 + i\omega\tau}\,\mathrm{d}\tau, \tag{67}$$

where σ_s^∞ is the high-frequency surface conductivity and σ_s^0 is the low-frequency surface conductivity. Both σ_s^∞ and σ_s^0 are real parameters. The function $f(\tau)$ represents the distribution of the relaxation times. It is normalized such that

$$\int_0^\infty f(\tau)\,\mathrm{d}\tau = 1. \tag{68}$$

In the case of a single relaxation time $f(\tau) = \delta(\tau - \tau_0)$, we recover the Debye distribution. The complex surface conductivity can be written as

$$\sigma_s^*(\omega) = \sigma_s'(\omega) + i\sigma_s''(\omega). \tag{69}$$

In the case of a Debye distribution, the real and imaginary parts of the surface conductivity are given by

$$\sigma_s'(\omega) = \sigma_s^\infty + \left(\sigma_s^0 - \sigma_s^\infty\right) \int_0^\infty \frac{f(\tau)}{1 + \omega^2\tau^2}\,\mathrm{d}\tau, \tag{70}$$

$$\sigma_s'(\omega) = \sigma_s^\infty + \frac{(\sigma_s^0 - \sigma_s^\infty)}{1 + \omega^2\tau_0^2}, \tag{71}$$

$$\sigma_s''(\omega) = \left(\sigma_s^\infty - \sigma_s^0\right)\omega \int_0^\infty \frac{\tau f(\tau)}{1 + \omega^2\tau^2}\,\mathrm{d}\tau, \tag{72}$$

and

$$\sigma_s''(\omega) = \frac{(\sigma_s^\infty - \sigma_s^0)\omega\tau_0}{1 + \omega^2\tau_0^2}. \tag{73}$$

If we return to the mechanistic model developed in Section 3.1, we can identify the parameters

$$\sigma_s^0 = \frac{2}{a_0}\Sigma_S^0 \tag{74}$$

and

$$\sigma_s^\infty = \frac{2}{a_0}\left(\Sigma_S^0 + \Sigma_S^\infty\right). \tag{75}$$

A special form of relaxation time distribution is the Cole–Cole distribution

$$\sigma_s^* = \sigma_s^\infty + \frac{\sigma_s^0 - \sigma_s^\infty}{1 + (i\omega\tau_0)^\alpha}, \tag{76}$$

where α is an empirical exponent called the Cole–Cole exponent. In the limit $\alpha = 1$, we recover the Debye distribution. The probability distribution of the relaxation time for a Cole–Cole distribution is given by [49]

$$f(\tau) = \frac{1}{2\pi}\frac{\sin[\pi(\alpha - 1)]}{\cosh[\alpha\ln(\tau/\tau_0)] - \cos[\pi(\alpha - 1)]}. \tag{77}$$

This distribution is symmetric about $\tau = \tau_0$. For $0.5 \leqslant \alpha \leqslant 1$, the Cole–Cole distribution looks like a log normal distribution. The tail of the Cole–Cole distribution is becoming increasingly broad as α decreases [47]. Consequently, the Cole–Cole distribution can be used to represent the approximate dispersion associated with a log normal distribution of grain size.

4. Maxwell–Wagner polarization

Theories of effective dielectric properties of composite media are based on the Maxwell approach [22]. Wagner [23] generalized Maxwell's theory in the case of dilute suspensions of spheres. The so-called differential self-consistent model [24] allows the determination of the final concentration of inclusions by addition of infinitesimal portions of inclusions $\delta\Phi$. The increment $\delta\sigma_n$ of the effective conductivity of the mixture due to the addition of an infinitesimal portion of inclusions $\delta\Phi_n$ is given by

$$\delta\sigma_n = 3\sigma_n\frac{\sigma_s - \sigma_n}{2\sigma_n + \sigma_s}\delta\Phi_n, \tag{78}$$

where σ_s is the electrical conductivity of the particle. After integrating from $\sigma_n = \sigma_f$ and $\Phi_n = 0$ to $\sigma_n = \sigma$ and $\Phi_n = 1 - \varphi$ with φ the porosity of the medium, we obtain the conductivity of the mixture σ [24]:

$$\frac{\sigma - \sigma_s}{\sigma_f - \sigma_s}\left(\frac{\sigma_f}{\sigma}\right)^{1/3} = \varphi. \tag{79}$$

This equation was extended by Hanai [25] to model the complex electrical conductivity of a porous granular composite:

$$\frac{\sigma^* - \sigma_s^*}{\sigma_f^* - \sigma_s^*}\left(\frac{\sigma_f^*}{\sigma^*}\right)^{1/3} = \varphi, \tag{80}$$

$\sigma^* = \sigma + i\omega\varepsilon$ represents the total conductivity function proposed by Dias [50] and De Lima and Sharma [29] (Appendix A).

For nonspherical grains, Eq. (80) is generalized by [26,51]

$$\frac{\sigma^* - \sigma_s^*}{\sigma_f^* - \sigma_s^*}\left(\frac{\sigma_f^*}{\sigma^*}\right)^{D} = \varphi, \tag{81}$$

where D is the polarization exponent, which depends on the shape of the solid grains. The total conductivity response of a two-phase mixture consisting of rock grains and pore solution

is given by

$$\sigma^* = \frac{\sigma_f^*}{F}\left(\frac{1-\sigma_s^*/\sigma_f^*}{1-\sigma_s^*/\sigma^*}\right)^m \tag{82}$$

and

$$F = \varphi^{-m}, \tag{83}$$

where $m = 1/(1-D)$ is called the cementation or Archie exponent. Equation (82) is consistent with the electrical conductivity σ^* of a pack of grains saturated by a solution of conductivity σ_f^* given by [52]:

$$\sigma^* = \frac{\sigma_f^*}{F}. \tag{84}$$

The exponent m depends on the shape of the grains. It is equal to 1.5 for spherical grains and it takes values >1.5 for nonspherical grains [26,51–55]. However, for loosely packed granular materials, m can be as low as 1.3. In our model, Eq. (82) is solved numerically with a Matlab routine.

The complex conductivity can be also written as

$$\sigma^* = \sigma_{\text{eff}} + i\omega\varepsilon_{\text{eff}}, \tag{85}$$

$$\sigma_{\text{eff}} = \text{Re}(\sigma^*), \tag{86}$$

and

$$\varepsilon_{\text{eff}} = \text{Im}(\sigma^*/\omega). \tag{87}$$

The phase of the complex conductivity response is defined by

$$\Theta = \arctan(\omega\varepsilon_{\text{eff}}/\sigma_{\text{eff}}). \tag{88}$$

In the following discussion, the absolute value of the phase of packs of glass beads will be given according to the definitions given in Appendix A.

A simulation of the phase response of a pack of glass beads is shown in Fig. 5 at different salinities. The first peak in the phase spectra corresponds to electrochemical polarization of the Stern layer around the grains and is directly sensitive to the grain size distribution. At higher frequencies, the response is dominated by the Maxwell–Wagner polarization. The comparison with the experimental data in the next section will also evidence electrochemical polarization associated with second-order heterogeneities in our opinion corresponding to the roughness of the surface of the grains. The effect of the roughness of the grains upon the phase spectra is situated in a frequency band that is usually intermediate between the polarization of the grains and the MW polarization.

5. Comparison with experimental data

We performed seven experiments with four samples of glass beads pack of different size and roughness and at different salinities. The experimental setups and results are displayed in Figs. 6–15 and summarized in Table 1. We first test the present model with experimental data obtained with one pack of glass beads of size 40–120 μm. Their chemical composition is $SiO_2 \sim 60.5\%$, $Na_2O \sim 12$–18%, $CaO \sim 5$–12%, $MgO \sim 4\%$,

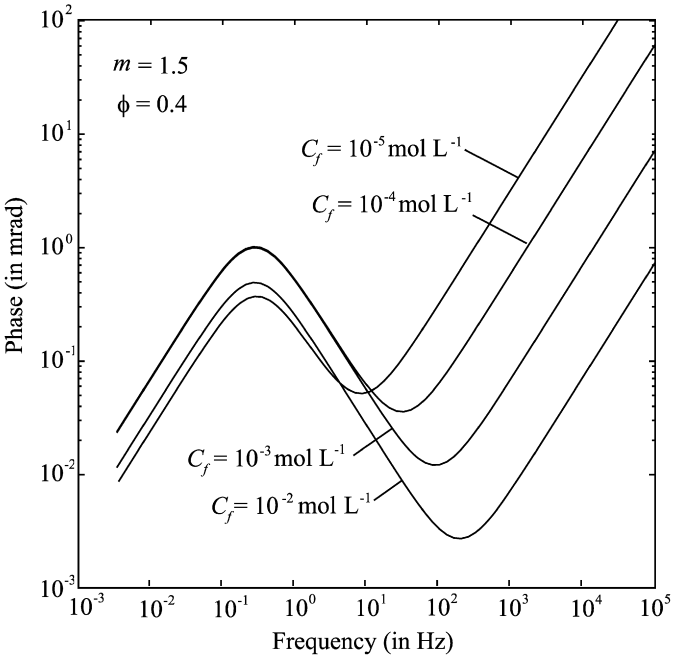

Fig. 5. Simulation of the response of a pack of glass beads (with no roughness of the grains) for four different salinities using the TLM model discussed in Section 2. The low-frequency peak corresponds to the polarization of the grains. The increase of the phase at higher frequencies corresponds to the Maxwell–Wagner polarization. We have assumed a log normal distribution for the PSD.

and $Al_2O_3 \sim 1\%$. They have electrochemical properties very similar to those of pure silica [56].

When the glass beads are in contact with water, the pH of the pore water is observed to increase. For example, we put 64 g of deionized water in contact with 255 g of these washed glass beads. The pH and the conductivity of the pore water reach values of 8.95 and 55×10^{-4} S m^{-1} after 45 min. Another experiment was performed by putting 111 g of deionized water in contact with 250 g of washed glass beads. The pH reaches a value of 9.24 and the pore water conductivity reaches a value of 1.03×10^{-2} S m^{-1} after 1 week. Results from the evolution of the composition of the pore water are reported in Table 2. The dominating cation resulting from the dissolution of the grains is sodium. The elevation of the electrical conductivity is probably related to the dissolution of the glass beads. This dissolution process brings cations constituting the glass beads to the solution. As a result, water dissociates to ensure electrical neutrality of the electrolyte and the electrical conductivity of the solution increases. This leads also to an increase of the concentration of hydroxide anions and to an elevation of the pH of the solution with time.

The experimental setup used to perform the first spectral-induced polarization experiment is shown in Fig. 6. Four nonpolarizing electrodes are inserted in a box filled with the pack of glass beads and the geometrical factor is determined using the box filled with the electrolyte NaCl at a given electrical conductivity. The array is the Wenner-α array (the two electrodes used to measure the difference of electrical potential are the inner electrodes and the two other electrodes are used to inject

Table 1
Summary of the results of the seven experiments

Experiment	C_f (in mol L^{-1})	a_0 (μm)	Du (dimensionless)	Γ_i^S (10^{16} m^{-2})	Γ_i^d (10^{16} m^{-2})
1	4×10^{-4}	35	0.66	6.5	7.5
2	1.1×10^{-3}	187.5	0.24	5.5	3.0
3 and 4	2×10^{-3}	187.5	0.06	6.0	2.3
5	1.3×10^{-3}	187.5	0.11	6.0	2.9
6	1.8×10^{-3}	187.5	0.08	6.0	2.5
7	3.1×10^{-3}	187.5	0.05	6.0	1.8

Salinity, C_f; peak of the grain size distribution, a_0; Dukhin number, Du (defined by $Du = \sigma_s'/\sigma_f$); density of the counterions in the Stern layer, Γ_i^S; density of the counterions in the diffuse layer, Γ_i^d. In the text, the word "sample" is used to describe a couple "glass bead" and "electrolyte." There are actually only three different glass beads used in our experiments: glass beads of size 1 (sample 1), glass beads of size 2 with rough surface (sample 2), and glass beads of size 2 with smooth surface (sample 3).

Table 2
Evolution of the composition of the pore water in contact with the glass beads (pack 1) at two different time lapses

Species	Concentration (in mol/L) (45 min)	Concentration (in mol/L) (1 week)
Ca^{2+}	1.8×10^{-4}	1.75×10^{-4}
K^+	7.7×10^{-6}	5.1×10^{-6}
Mg^{2+}	4.11×10^{-5}	4.11×10^{-5}
Na^+	4.48×10^{-4}	8.2×10^{-4}
Al^{3+}	3.1×10^{-6}	2.76×10^{-6}
pH	8.95	9.24
SiO_2	5×10^{-4}	1.04×10^{-3}

In the first case, 255 g of glass beads were put in contact with 64 g of deionized water for 45 min. The mixture was in contact with the atmosphere. In the second case, 250 g of glass beads were put in contact with 111 g of deionized water (the gas is nitrogen). Chemistry is determined after 1 week.

the electrical current). This insures a high signal-to-noise ratio. In addition, we checked that the drift of the electrodes can be neglected. Spectral induced polarization (SIP) measurements were performed with the SIP-Fuchs system operating in the frequency range 10^{-1}–10^4 Hz (see http://www.radic-research.de/Flyer_SIP-Fuchs_II_151104.pdf).

Given the chemical composition of the glass beads and the kinetics associated with the dissociation of Na_2O, the major cationic constituent of the solution is sodium. However, Ca^{2+} and Mg^{2+} may be present in nonnegligible quantities compared to the quantity of sodium. These cations have similar ionic mobilities in solution (5.19×10^{-8} m^2 s^{-1} V^{-1} for Na^+, 6.16×10^{-8} m^2 s^{-1} V^{-1} for Ca^{2+}, and 5.48×10^{-8} m^2 s^{-1} V^{-1} for Mg^{2+} [27]). Therefore the peaks associated with the spectrum of the phase, at low frequencies, would be located at the same characteristic frequency (see Eq. (50)). As in Revil and Leroy [44], we assume that the value of the partition coefficient f_Q in the case of a binary monovalent electrolyte is similar to its value for a multiionic electrolyte. In the case of a smectite mineral immersed in a multiionic solution and at high ionic strength Leroy et al. [33] found a value of f_Q equal to 0.94. This value is not too far from the value calculated by Leroy and Revil [38] (0.98) for the same mineral but in the case of a binary monovalent electrolyte such as NaCl or KCl.

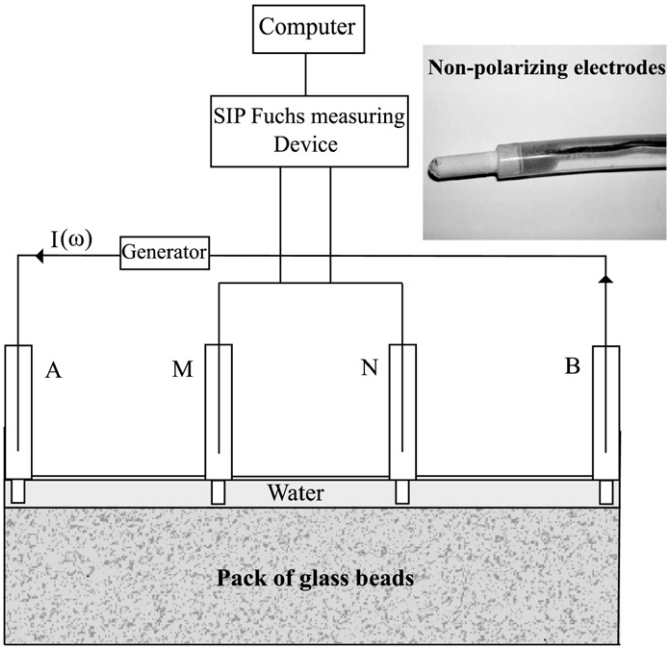

Fig. 6. Sandbox used for the spectral induced polarization (SIP) experiment. We use four Cu/$CuSO_4$ nonpolarizing electrodes with the Wenner-α configuration. The geometrical factor used to convert the conductance to conductivity is determined from a similar experiment using an electrolyte of known conductivity. The current at a given frequency is injected through the outer electrodes (A, B), and the inner electrodes (M, N) measure the electrical field associated with the polarization of the porous medium. The length of the sandbox is 30 cm and its width is 20 cm.

The measured pH of the solution was 9.0 and the electrical conductivity of the solution (at 25 °C) was equal to 5×10^{-3} S m^{-1}.

The phase measurements and the model response as a function of the frequency are plotted in Fig. 8. Taking $D_S = 2.45 \times 10^{-9}$ m^2 s^{-1} and $a_0 = 35$ μm, the critical frequency for the electrochemical polarization is equal to 2 Hz (inverse of the relaxation time calculated by Eq. (50)), which corresponds to the peak of the first relaxation observed in Fig. 8. At frequencies higher than 1 kHz, the response of the medium is dominated by the MW polarization. However, above 1 kHz, the measured phase data are also likely to be contaminated by coupling effects associated with the wire layout of the experimental setup and overlapping with the Maxwell–Wagner polarization.

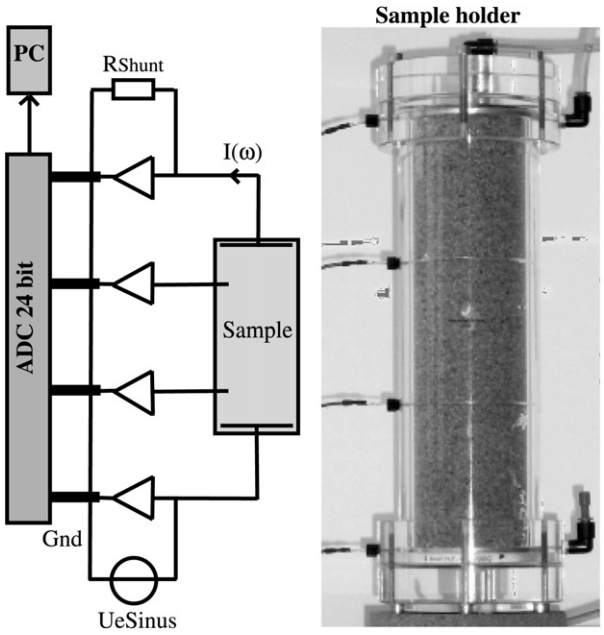

Fig. 7. Second experimental setup used for the measurements. The employed cylindrical sample holder has a length of 30 cm and an inner diameter of 6 cm. A four-electrode array consisting of two outer current electrodes (porous bronze plates with an effective pore diameter of 15 μm) and two inner potential electrodes (silver rings fixed in grooves 10 cm apart) is used.

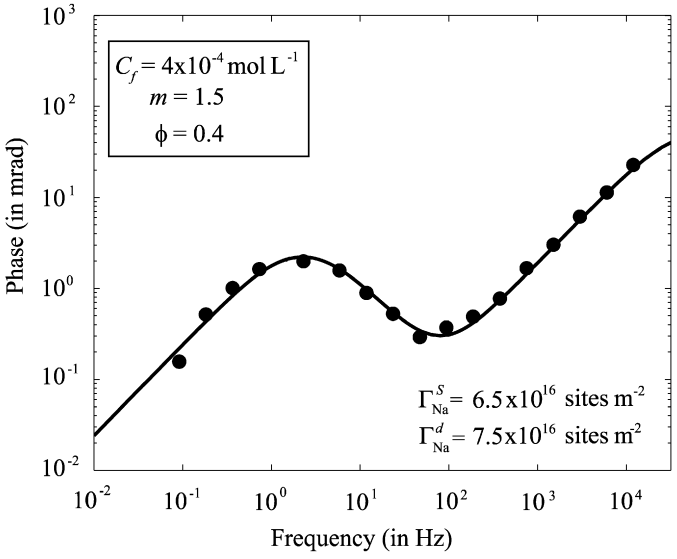

Fig. 8. Measured (filled circles) and calculated (solid line) angular frequency ω dependence of the phase of a pack of glass beads (sample 1). Measured porosity 0.40; pH (measured) 9.0. The cementation exponent ($m = 1.5$) is determined from electrical conductivity measurements [56]. The salinity of the pore solution used in the model is equal to 4×10^{-4} mol L^{-1} and the electrical conductivity is 5×10^{-3} S m^{-1} which corresponds to the measured electrical conductivity. Parameters determined from the TLM model: density of the counterions in the diffuse layer (7.5×10^{16} counterions m^{-2}) and density of the counterions in the Stern layer (6.5×10^{16} counterions m^{-2}). We use $D_S = 2.45 \times 10^{-9}$ m s^{-1}.

The mean particle diameter was determined with a laser granulometer (Laser Scattering Mastersizer MALVERN operating in the range 50 nm–2 mm; Fig. 9). The PSD shows the

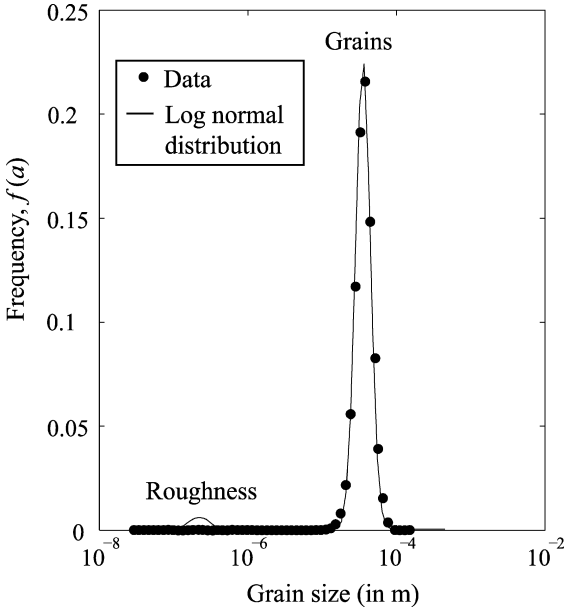

Fig. 9. Particle size distribution of the investigated glass beads pack (sample 1) determined using a laser granulometer. The solid line represents a fit of the data with two log normal distributions (mean grain radius $a_0 = 35$ and 0.2 μm).

main distribution in the range 20–50 μm. The particle size distribution (shown in Fig. 9) is fitted with the following log normal distribution,

$$f(a) = \frac{1}{\sqrt{2\pi}\hat{\sigma}} \exp\left\{-\left[\frac{\log(a/a_0)}{\sqrt{2}\hat{\sigma}}\right]^2\right\}, \tag{89}$$

with $a_0 = 35$ μm corresponding to the first peak of the PSD and $\hat{\sigma} = 0.1$ as the standard deviation. The roughness is described by a second log normal distribution and the parameters of this second distribution are fitted to the phase data. The second peak may be caused by the formation of silica gel layers at the surface of the mineral created at pH > 8 [62] and by other heterogeneities at the surface of the glass beads. The measured mass density of the grains is 2430 kg m^{-3} and the measured porosity of the various packs used in this study is $\varphi = 0.40$ [56] irrespective of their grain sizes.

A comparison between our model and the experimental data is shown in Fig. 8. The porosity, the salinity, and the pH are measured, the value of the cementation exponent ($m = 1.5$) is assumed, and the values of the parameters describing the log normal distribution associated with the roughness of the grains are fitted to the data assuming that the roughness of the grains is described by a single log normal distribution. There is a good agreement between the model and the experimental data over the frequency range investigated. Note that this can be achieved only if the mobility of the counterions in the Stern layer is equal to the mobility of the counterions in the diffuse layer. This is in agreement with the results obtained by Lesmes and Morgan [47] using spectral induced polarization data and Tarasov and Titov [57] using time-domain induced polarization data.

Experiments 2 to 7 were performed on glass beads of size 250–500 μm using the experimental setup shown in Fig. 7 (see [5]). The used instrumentation, developed at the Central

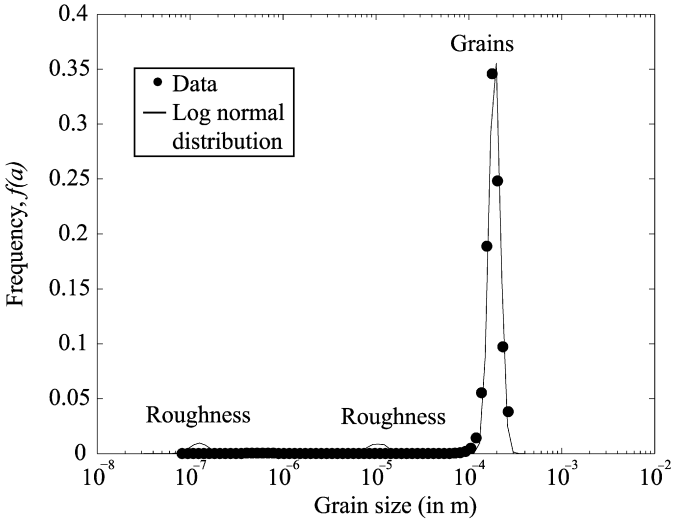

Fig. 10. Particle size distribution of the investigated glass beads pack (sample 2) determined using a laser granulometer. The solid line represents a fit of the data with a log normal distribution plus two small log normal distributions to include the effect of the roughness of the grains.

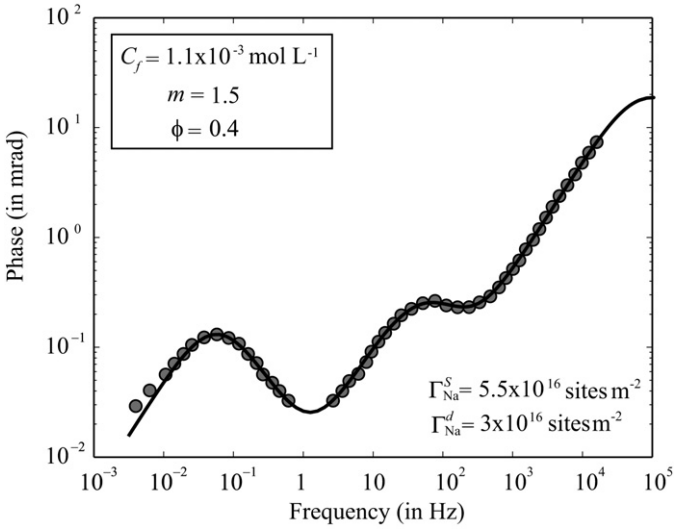

Fig. 11. Measured (filled circles) and calculated (solid line) angular frequency ω dependence of the phase of a pack of glass beads (sample 2). Measured porosity 0.40; pH (measured) 9.2; we assume $m = 1.5$. The salinity of the pore solution used in the model is equal to 1.1×10^{-3} mol L^{-1} and the electrical conductivity is 1.5×10^{-2} S m^{-1} which corresponds to the measured electrical conductivity. Parameters determined from the TLM model: density of the counterions in the diffuse layer (3×10^{16} counterions m^{-2}) and density of the counterions in the Stern layer (5.5×10^{16} counterions m^{-2}). We use $D_S = 2.45 \times 10^{-9}$ m s^{-1}.

Laboratory for Electronics (ZEL) at the Forschungszentrum Jülich (Germany), offers a broader measurement spectrum (1 mHz–45 kHz) and a higher phase accuracy (below 1 kHz better than 0.1 mrad) [5] than the device used in experiment 1. The glass beads were put initially with deionized water and remained 1 to several weeks in a closed box. The samples of glass beads have the following chemical composition: 72% SiO_2, 14% Na_2O, 9% CaO, 4% MgO, and 1% Al_2O_3. The SIP measurements were done at the laboratory Agrosphere (ICG 4) at the Forschungszentrum Jülich (Germany). The employed cylindrical sample holder has a length of 30 cm and an inner diameter of 6 cm (Fig. 7). A four-electrode array consisting of two outer current electrodes (porous bronze plates with an effective pore diameter of 15 μm) and two inner potential electrodes (silver rings fixed in grooves 10 cm apart) is used. The measuring system was in particular tested on electrical networks [5] with phase responses in a range typical of sedimentary rocks.

Fig. 10 shows the particle size distribution of the second sample (glass beads with rough surface) measured by a laser granulometer. The phase angle distribution is shown in Fig. 11. The agreement between simulated and measured phase spectra (taking into account a parasitic capacitance of 0.5 pF) is very good, even for phase values much below 1 mrad. The measured pH of the solution was 9.2 and the measured electrical conductivity of the solution (at 25 °C) was equal to 1.5×10^{-2} S m^{-1} (the glass beads remained 2 weeks in a closed sample holder). For the second sample, the peak of the PSD is at 1.875×10^{-4} m (187.5 μm). Taking $D_S = 2.45 \times 10^{-9}$ m^2 s^{-1} and $a_0 = 187.5$ μm, the critical frequency for the electrochemical polarization is equal to 75 mHz, which corresponds to the peak of the first relaxation observed in Fig. 11 (first peak at ~70–80 mHz). The peak of the second maximum is situated at a critical frequency ω_c approximately equal to 80 Hz. Using $a_0 = (2D_i^S/\omega_c)^{1/2}$, this would correspond to heterogeneities with a size of 6 μm. These heterogeneities correspond very well

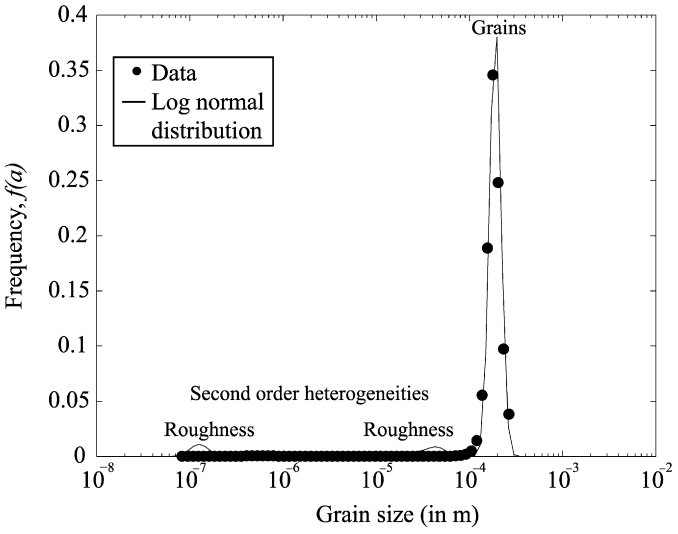

Fig. 12. Particle size distribution of the investigated glass beads pack determined using a laser granulometer (sample 3). The solid line represents a fit of the data with a log normal distribution plus two small log normal distributions to include the effect of the roughness of the grains.

to the size of the roughness at the surface of the grains (see Fig. 15).

In the third experiment (glass beads with smooth surface), the pH of the solution was measured at 9.3 and the electrical conductivity of the solution determined experimentally (at 25 °C) was equal to 2.6×10^{-2} S m^{-1} (the glass beads remained 3 weeks in a closed box). The grain size distribution of sample 3 is reported in Fig. 12. The surface of the beads is smooth, with a small roughness. The measured phase spectrum is shown in Fig. 13. For sample 3, taking $D_S = 2.45 \times 10^{-9}$ m^2 s^{-1} and

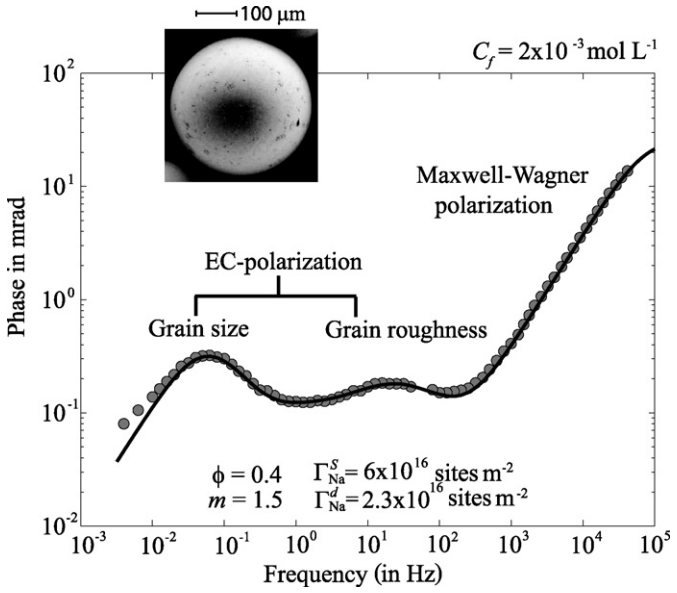

Fig. 13. Measured (filled circles) and calculated (solid line) angular frequency ω dependence of the phase of a pack of smooth glass beads (sample 3). Measured porosity 0.40; pH (measured) 9.3; we assume $m = 1.5$. The salinity of the pore solution used in the model is equal to 2×10^{-3} mol L^{-1} and the electrical conductivity is 2.6×10^{-2} S m^{-1} which corresponds to the measured electrical conductivity. Parameters determined from the TLM model: density of the counterions in the diffuse layer (2.3×10^{16} counterions m^{-2}) and density of the counterions in the Stern layer (6×10^{16} counterions m^{-2}). The picture shows the size of the glass beads and their roughness. The beads are relatively smooth.

$a_0 = 187.5$ µm, the critical frequency for the electrochemical polarization is equal to 75 mHz (as for sample 2). This value is close to the value of the frequency corresponding to the peak of the first relaxation observed in Fig. 13 (first peak at a critical frequency of ∼70–80 mHz). The second peak is around 20 Hz and corresponds to heterogeneity of the size of 12 µm. This is the size of the heterogeneities associated with the roughness of the grains (Fig. 13).

Fig. 14 presents a comparison of the phase spectra of packs of glass beads with smooth and rough surfaces (samples 3 and 4; sample 4 was treated with an acid to increase the roughness of the surface of the beads). In the case of the beads pack with a rough surface, the second peak of the phase spectrum is almost as high as the first peak. Fig. 14 shows very well the effect of the roughness upon the phase spectra and especially the increase of the amplitude of the second peak when roughness increases.

The grain size distribution and phase data corresponding to beads pack with rough surfaces (sample 4) are reported in Fig. 15. The measurements were realized at three different ionic strengths. The electrical conductivities of the solution were measured as 1.7×10^{-2} S m^{-1} (pH 9.2), 2.3×10^{-2} S m^{-1} (pH 9.3), and 4.1×10^{-2} S m^{-1} (pH 9.5). Our model is able to reproduce the experimental data quite well by accounting for the effect of the strong roughness of the glass beads. Note that the agreement between the data and the model decreases at very low frequency ($<10^{-2}$ Hz). This is due probably to the multi-ionic character of the solution and/or electrode effects in the phase measurements. As shown in Fig. 4 the predictions of the

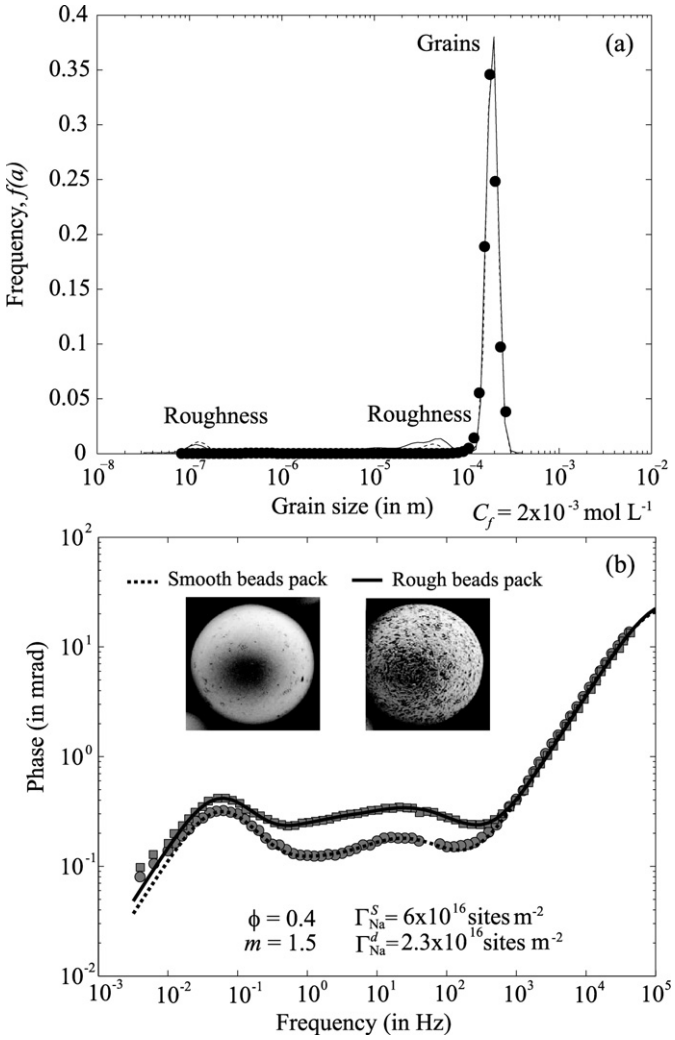

Fig. 14. Measured (filled circles) and calculated (solid and dashed lines) grain size (a) and phase (b) for smooth and rough glass beads (samples 3 and 4). The measured porosity is 0.40 and the measured pH is 9.3 for an electrical conductivity of 2.6×10^{-2} S m^{-1}. We assume $m = 1.5$. Parameters determined from the TLM model: density of the counterions in the diffuse layer (2.3×10^{16} counterions m^{-2}) and density of the counterions in the Stern layer (6×10^{16} counterions m^{-2}).

TLM concerning the partition of the counterions between the Stern and the diffuse layers are in agreement with the values calculated by the SIP model. The partition coefficient increases with the ionic strength and with the pH. Spectral induced polarization seems to offer the possibility to monitor nonintrusively ongoing dissolution of a mineral surface and the concomitant variation of the roughness of this surface.

6. Concluding statements

A low-frequency polarization model of water-saturated granular media accounting for both the electrochemical polarization of the Stern layer and the Maxwell–Wagner polarization is developed. The electrochemical polarization is connected to the properties of the electrical triple layer coating the surface of the grains and especially to the partition coefficient of the counterions between the Stern and the diffuse layers. The elec-

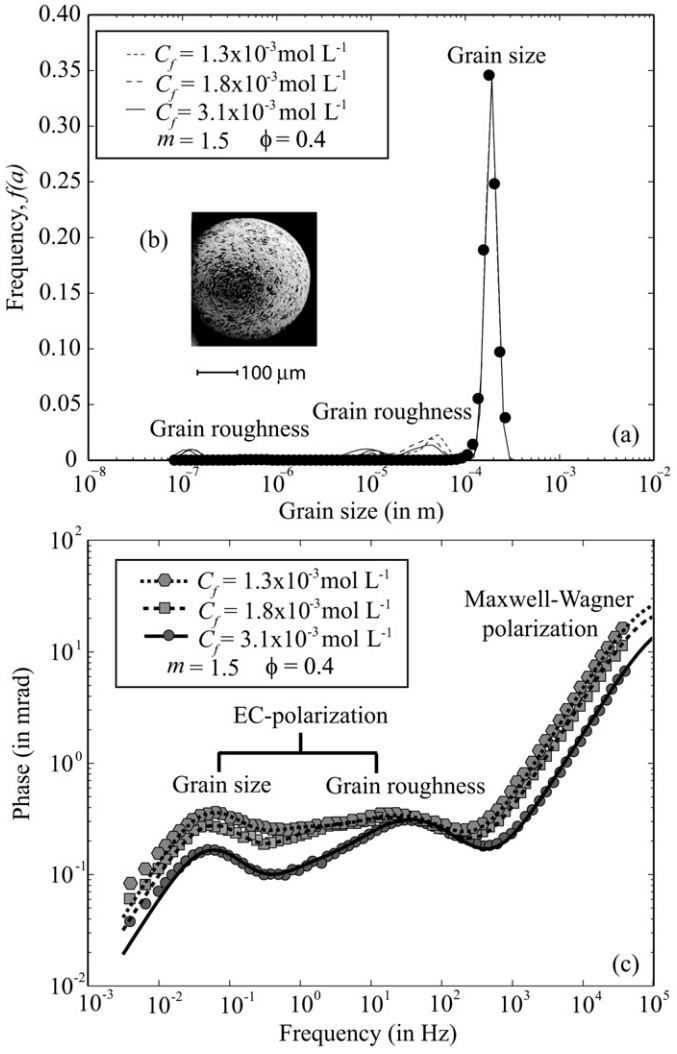

Fig. 15. Measured (filled circles) and calculated (solid and dashed lines) grain size (a) and phase (c) of a pack of rough glass beads (sample 4). The measured porosity is 0.40 and the measured pH is variable and depends on the ionic strength of the solution: 9.2 for an electrical conductivity of 1.7×10^{-2} S m^{-1}, 9.3 for $\sigma_f = 2.3 \times 10^{-2}$ S m^{-1}, and 9.5 for $\sigma_f = 4.1 \times 10^{-2}$ S m^{-1}. We assumed $m = 1.5$. Parameters were determined from the TLM model (see the values of the densities of counterions in Table 1). The picture (b) shows the size of the glass beads and their strong roughness. The size of the heterogeneities at the surface of the grains is on the order of 10 µm and smaller.

trochemical polarization is controlled by the Stern layer. The polarization of the diffuse layer is neglected because of the connectivity of the diffuse layers at the macroscopic scale and therefore the diffuse layer has only a DC conductivity contribution. We consider also the DC conductivity contribution from the protons of the water adsorbed onto the mineral surface. It follows that surface conductivity of the grains is frequency dependent with a relaxation time that depends on the size of the grain. For a grain size distribution given by a log normal distribution, we use a Cole–Cole distribution to represent the influence of the grain size distribution upon the distribution of the relaxation times. In the general case, we can use the superposition principle and therefore a convolution product between the particle size distribution and the response of a single grain. The Maxwell–Wagner polarization is accounted for by using the differential effective medium theory at the scale of a representative elementary volume of the porous material. Comparisons of the phase spectra of infiltrated glass beads are successful assuming that the mobility of the counterions is the same in the Stern layer and in the diffuse layer. The model implies that the partition coefficient of the counterions in the electrical triple layer increases with the salinity of the pore water in agreement with TLM calculations.

Acknowledgments

This work was supported by the NSF (Contract NSF-0710949), the GDR-FORPRO, the French National Agency for Radioactive Waste Management (ANDRA), and ANR-CNRS-INSU-ECCO. The post-doctoral grant of P. Leroy was supported by ANDRA. This is contribution FORPRO 2007/11 A. We thank T. Conte (BRGM) for the geochemical measurements and A. Lassin for fruitful discussions. Moreover, we are grateful to a number of colleagues at the Forschungszentrum Jülich, in particular Odilia Esser (ICG 4), who assisted with the spectral induced polarization measurements, Oliver Kranendonck (formerly ICG 5), who performed the laser granulometric measurements, Walter Schröder (ICG 3) and Hans-Martin Münch (formerly ICG 4), who provided the scanning electron microscope images, and Egon Zimmermann and Walter Glaas (both ZEL), who helped optimizing the SIP data acquisition.

Appendix A

Ampère's law is written as [22],

$$\nabla \times \mathbf{H} = \mathbf{j} + \frac{\partial \mathbf{D}}{\partial t}, \tag{A.1}$$

where t is time (in s), $\mathbf{j}$ is the electrical current density (in A m^{-2}), $\mathbf{H}$ is the magnetic field intensity (in A m^{-1}), and $\mathbf{D} = \varepsilon \mathbf{E}$ is the dielectric displacement (in C m^{-2}). We neglect the streaming current density in the expression of the current density and therefore the current density is given by Ohm's law ($\mathbf{j} = \sigma \mathbf{E}$) and we assume that the electrical field is given by

$$\mathbf{E} = \mathbf{E}_0 \exp(i\omega t) \tag{A.2}$$

(engineer's convention). According to Eq. (A.1), the current density is the sum of a conduction current plus a displacement current. It follows that the total current density is given by

$$\mathbf{J}_t = (\sigma + i\omega\varepsilon)\mathbf{E}, \tag{A.3}$$

where σ and ε are complex scalars dependent upon frequency, $\sigma = \sigma' + i\sigma''$ and $\varepsilon = \varepsilon' + i\varepsilon''$ (with the sign convention taken from Fuller and Ward [58] and Keller [59]) in an isotropic medium (note that Olhoeft [60] used a different sign convention, $\sigma = \sigma' + i\sigma''$ and $\varepsilon = \varepsilon' - i\varepsilon''$, because with this convention σ', σ'', ε', and ε'' have positive values). The total current density can be written as

$$\mathbf{J}_t = \sigma^* \mathbf{E}, \tag{A.4}$$

where $\sigma^* = \sigma_{\text{eff}} + i\omega\varepsilon_{\text{eff}}$ is the total current conductivity function and σ_{eff} and ε_{eff} are real scalars dependent upon frequency. These effective parameters are the parameters that are measured during an experiment. It follows that $\sigma_{\text{eff}} = \sigma' - \omega\varepsilon''$ and $\varepsilon_{\text{eff}} = \varepsilon' + \sigma''/\omega$ (note that $-\omega\varepsilon''$ is always positive). Therefore the effective conductivity includes contributions from charge conduction and polarization mechanisms. Similarly, the effective permittivity has contributions from both conduction and polarization.

References

[1] G.R. Olhoeft, Geophysics 50 (1985) 2492–2503.
[2] L. Slater, D. Lesmes, Geophysics 67 (2002) 77–88.
[3] O.A.L. De Lima, Geophysics 58 (1992) 1689–1702.
[4] F. Börner, J.R. Schopper, A. Weller, Geophys. Prospect. 44 (1996) 583–601.
[5] A. Kemna, H.-M. Münch, K. Titov, E. Zimmermann, H. Vereecken, Extended Abstracts "Near Surface 2005", 11th European Meeting of Environmental and Engineering Geophysics, Eur. Assn. Geosci. Eng., 2005, P054, 4 pp;
A. Kemna, A. Binley, L. Slater, Geophysics 69 (2004) 97–107;
E. Zimmermann, H.-M. Münch, J. Berwix, W. Glaas, H. Meier, A. Kemna, in: U. Brill, D.U. Sauer (Eds.), Impedanzspektroskopie—Grundlagen und Anwendungen, Sonderausgabe Technische Mitteilungen, vol. 99 (1/2), Organ des Haus der Technik e. V., Essen, 2006, pp. 244–249.
[6] F. Börner, M. Gruhne, J. Schön, Geophys. Prospect. 41 (1993) 83–98.
[7] H.P. Schwan, G. Schwarz, J. Maczuk, H. Pauly, J. Phys. Chem. 66 (1962) 2626–2635.
[8] C. Ballario, A. Bonincontro, C. Cametti, J. Colloid Interface Sci. 54 (1976) 415–423.
[9] J.P. Poley, J.J. Nooteboom, P.J. deWaal, Log Analyst 19 (1978) 8–30.
[10] N.C. Lockhart, J. Colloid Interface Sci. 74 (1980) 509–519.
[11] V.N. Shilov, A.V. Delgado, F. Gonzalez-Caballero, C. Grosse, Colloids Surf. A Physicochem. Eng. Aspects 192 (2001) 253–265.
[12] K.S. Cole, R.H. Cole, J. Chem. Phys. 9 (1941) 341–351.
[13] D.W. Davidson, R.H. Cole, J. Chem. Phys. 19 (12) (1951) 1484–1490.
[14] A.K. Jonscher, Dielectric Relaxation in Solids, Chelsea Dielectric, London, 1983.
[15] G. Schwarz, J. Phys. Chem. 66 (1962) 2636–2642.
[16] J.M. Schurr, J. Phys. Chem. 68 (1964) 2407–2413.
[17] S.S. Dukhin, V.N. Shilov, Dielectric Phenomena and the Double Layer in Disperse Systems and Polyelectrolytes, John Wiley and Sons, New York, 1974.
[18] M. Fixman, J. Phys. Chem. 72 (1980) 5177–5186.
[19] J. Lyklema, S.S. Dukhin, V.N. Shilov, J. Electroanal. Chem. 143 (1983) 1–21.
[20] R.W. O'Brien, J. Colloid Interface Sci. 92 (1) (1983) 204–216.
[21] E.J. Hinch, J.D. Sherwood, W.C. Chen, P.N. Sen, J. Chem. Soc. Faraday Trans. 2 (80) (1984) 535–551.
[22] J.C. Maxwell, A Treatise on Electricity and Magnetism, third ed., Oxford University Press, London, 1892.
[23] K.W. Wagner, Arch. Elektrotechn. 2 (1914) 371–387.
[24] D.A.G. Bruggeman, Annal. Phys. 24 (1935) 636–679.
[25] T. Hanai, in: P. Sherman (Ed.), Emulsions Science, Academic Press, New York, 1968, pp. 354–477.
[26] P.N. Sen, C. Scala, M.H. Cohen, Geophysics 46 (1981) 781–795.
[27] A. Revil, L.M. Cathles, S. Losh, J.A. Nunn, J. Geophys. Res. 103 (B10) (1998) 23925–23936;
A. Revil, D. Hermitte, E. Spangenberg, J.J. Cochémé, J. Geophys. Res. 107 (B8) (2002) 2168.
[28] A. Revil, J. Geophys. Res. 105 (B7) (2000) 16749–16768.
[29] O.A.L. De Lima, M.M. Sharma, Geophysics 57 (3) (1992) 431–440.
[30] A.L. Endres, R.J. Knight, J. Colloid Interface Sci. 157 (2) (1993) 418–425.
[31] A. Kitamura, K. Fujiwara, T. Yamamoto, S. Nishikawa, H. Moriyama, J. Nuclear Sci. Technol. 36 (12) (1999) 1167–1175.
[32] A. Revil, P.W.J. Glover, Phys. Rev. B 55 (3) (1997) 1757–1773;
A. Revil, P.W.J. Glover, Geophys. Res. Lett. 25 (5) (1998) 691–694.
[33] P. Leroy, A. Revil, S. Altmann, C. Tournassat, Geochim. Cosmochim. Acta 71 (5) (2007) 1087–1097.
[34] T. Hiemstra, W.H. Van Riemsdijk, J. Colloid Interface Sci. 136 (1990) 132–150.
[35] E. Papirer, Adsorption on Silica Surfaces, Marcel Dekker, New York, 2000.
[36] R.J. Hunter, Zeta Potential in Colloid Science: Principles and Applications, Academic Press, New York, 1981.
[37] A. Szymczyk, P. Fievet, A. Foissy, J. Colloid Interface Sci. 255 (2002) 323–331.
[38] P. Leroy, A. Revil, J. Colloid Interface Sci. 270 (2) (2004) 371–380.
[39] C.G. Armistead, A.J. Tyler, F.H. Hambleton, S.A. Mitchell, J.A. Hockey, J. Phys. Chem. 73 (11) (1969) 3947.
[40] M. Aydin, T. Yano, S. Kilic, Soil Sci. Soc. Am. J. 68 (2004) 450–459.
[41] J. Lyklema, J.T.G. Overbeek, J. Colloid Interface Sci. 16 (1961) 595–608.
[42] J.A. Davis, J.O. Leckie, J. Colloid Interface Sci. 67 (1) (1978) 90–107.
[43] G.H. Bolt, J. Phys. Chem. 61 (1957) 1166–1169.
[44] A. Revil, P. Leroy, J. Geophys. Res. 109 (2004) B03208;
A. Revil, P. Leroy, K. Titov, J. Geophys. Res. 110 (2005) B06202.
[45] C.T. O'Konski, J. Phys. Chem. 64 (1960) 605–619.
[46] D.G. Miller, J. Phys. Chem. 70 (8) (1966) 2639–2659.
[47] D.P. Lesmes, F.D. Morgan, J. Geophys. Res. 106 (B7) (2001) 13329–13346.
[48] J.R. Wait, Geoexploration 22 (1984) 107–127.
[49] C.J.F. Bötcher, P. Bordewijk, Theory of Electric Polarization, vol. II, Dielectrics in Time-Dependent Fields, Elsevier Science, 1978.
[50] C.A. Dias, J. Geophys. Res. 77 (1972) 4945–4956.
[51] K.S. Mendelson, M.H. Cohen, Geophysics 47 (2) (1982) 257–263.
[52] G.E. Archie, Trans. AIME 146 (1942) 54–61.
[53] A. Revil, N. Linde, J. Colloid Interface Sci. 302 (2006) 682–694.
[54] O.A.L. De Lima, M.M. Sharma, Soc. Prof. Well Log Analysts, 32nd Ann. Logging Symp., Paper G, 1991.
[55] W.E. Kenyon, Dielectric dispersion in laboratory measurements on cores, Schlumberger Wireline Interpretation Sym., 1983.
[56] A. Crespy, A. Bolève, A. Revil, J. Colloid Interface Sci. 305 (2007) 188–194.
[57] A. Tarasov, K. Titov, Geophys. J. Int. 170 (1) (2007) 31–43.
[58] B.D. Fuller, S.H. Ward, IEEE Trans. Geosci. Electron. GE-8 (1970) 7–18.
[59] G.V. Keller, in: M.N. Nabighian (Ed.), Electromagnetic Methods in Applied Geophysics, in: Soc. of Expl. Geophys., vol. 1, 1988, pp. 13–51.
[60] G.R. Olhoeft, in: Initial Report of the Petrophysics Laboratory, U.S. Geol. Survey, Circular 789, 1979, pp. 1–25.
[61] A.M. Gaudin, D.W. Fuerstenau, Trans. AIME (Am. Inst. Min. Metall. Petrol. Eng.) 202 (1955) 66–72.
[62] A. Revil, P. Pezard, P.W.J. Glover, J. Geophys. Res. 104 (B9) (1999) 20021–20031.
[63] C. Grosse, V.N. Shilov, J. Phys. Chem. 100 (1996) 1771–1778.